

Kohn–Sham inversion with mathematical guarantees

Michael F. Herbst,^{1,2,*} Vebjørn H. Bakkestuen,³ and Andre Laestadius^{3,4,†}

¹*Mathematics for Materials Modelling (MatMat),
Institute of Mathematics & Institute of Materials,*

École Polytechnique Fédérale de Lausanne, 1015 Lausanne, Switzerland

²*National Centre for Computational Design and Discovery of Novel Materials (MARVEL),
École Polytechnique Fédérale de Lausanne, 1015 Lausanne, Switzerland*

³*Department of Computer Science, Oslo Metropolitan University, 0130 Oslo, Norway*

⁴*Hylleraas Centre for Quantum Molecular Sciences, Department of Chemistry,
University of Oslo, P.O. Box 1033 Blindern, N-0315 Oslo, Norway*

We use an exact Moreau-Yosida regularized formulation to obtain the exchange-correlation potential for periodic systems. We reveal a profound connection between rigorous mathematical principles and efficient numerical implementation, which marks the first computation of a Moreau-Yosida-based inversion for physical systems. We develop a mathematically rigorous inversion algorithm including error bounds that are verified numerically in bulk silicon. This unlocks a new pathway to analyze Kohn–Sham inversion methods, which we expect in turn to foster mathematical approaches for developing approximate functionals.

Density-functional theory (DFT) simulations are an indispensable tool in chemistry, materials science and solid-state physics [1–3]. In this theory, the unknown is the electronic density $\rho(\mathbf{r})$ instead of the full many-body wavefunction, making computations substantially more tractable [4]. However, one of the key ingredients of DFT, the universal density functional, is not known explicitly [5]. One therefore usually employs the Kohn–Sham (KS) formulation [6], where all unknowns of DFT are collected into the exchange-correlation (xc) functional, which is subsequently approximated. Substantial work has been devoted to developing accurate xc functional approximations [7]. Although DFT is in principle exact, and despite significant advancements, KS-DFT still faces challenges in certain physical contexts. Notable difficulties include (a) accurately describing processes involving fractional electronic charge, such as dissociation or charge-transfer excitations [8–10], as well as (b) addressing the well-known band gap problem, where semiconductor band gaps are underestimated [11–15]. Developing better xc functional approximations thus remains a major research thrust [16]. One obstacle is a lack in mathematical understanding between the exact universal density functional and common approximations [3], making the rigorous construction of new and better functionals hard.

In this Letter we will focus on KS inversion [17–42], which has been suggested as a tool to aid the construction of xc functionals [36, 40, 42]. In contrast to the standard KS formulation, where one is equipped with the xc potential v_{xc} and determines the density from a variational principle (forward problem), KS inversion does the reverse: given a ground-state density one seeks the xc potential which reproduces the density in an auxiliary non-interacting setting. Unfortunately KS inversion is far less studied than the forward KS-DFT problem. Additionally, the development of a robust and efficient

numerical scheme for KS inversion remains an open challenge [40, 42–46].

In a recently established result [47], the xc potential has been obtained as a mathematical limit within the Moreau-Yosida (MY) regularized formulation of DFT [48–52]. This limit involves first finding the *proximal density* (of a ground-state density) and then utilizing the duality map between the density and potential spaces. This novel link is extremely promising as MY regularization deals with the non-differentiability of the exact universal functional [53]. Notably, for both the aforementioned fractional electronic charge as well as the band gap problems, a profound connection to the non-differentiability of KS-DFT has been established in early works on DFT [11, 12].

Here, we focus on periodic systems, a setting that is particularly suited to obtain an efficient numerical scheme for KS inversion that maintains the connection to a rigorous mathematical formulation. Employing the Density-Functional ToolKit (DFTK) [54], we are able to propose an implementation, which is capable of performing KS inversion on systems of practical relevance, such as bulk silicon. Notably, in the context of realistic physical systems, this is the first time a MY-based framework has been applied for KS inversion. Being equipped with a MY inversion procedure within a strict mathematical framework, we demonstrate how this inversion scheme opens up new insights into convergence properties and error analysis. In particular we develop first rigorous error bounds for inverse KS problems. This paves the way for improved numerical analyses of KS inversion and is expected to be a crucial element in the future development of density functionals.

The remainder of this Letter is structured as follows. First, we briefly present the mathematical framework of the MY inversion scheme within a periodic setting. We relate the proximal density to the xc potential v_{xc} and

present an error analysis including rigorous bounds based on the proximal mapping. Finally, the theory is numerically implemented to demonstrate the suitability of this scheme, including the error bounds, to realistic physical systems by applying it to bulk silicon.

Density-functional theory considers a system of N electrons subjected to a scalar potential $v(\mathbf{r})$. Let $E(v)$ denote the ground-state energy and $F(\rho)$ the *exact* universal functional computed from states that minimize all internal energy contributions under a density constraint. This approach can be viewed as an energy minimization problem: given an external potential v , find the corresponding density ρ such that $E(v) = F(\rho) + \langle v, \rho \rangle$. Here $\langle v, \rho \rangle$ is the dual pairing between $\rho \in \mathcal{D}$ and $v \in \mathcal{V} = \mathcal{D}^*$, where \mathcal{D} is a Banach space (complete normed space with norm $\|\cdot\|_{\mathcal{D}}$) and \mathcal{D}^* its dual (i.e., the space of bounded, linear functionals on \mathcal{D} with induced norm $\|\cdot\|_{\mathcal{V}}$). Employing a slightly different sign convention, E can be viewed as the Fenchel conjugate of F , and F as the conjugate of E . Finding the ground-state density is then Hohenberg–Kohn *variational principle* $E(v) = \inf_{\rho \in \mathcal{D}} \{F(\rho) + \langle v, \rho \rangle\}$ [55].

Next, we introduce the *Moreau–Yosida regularization* of a density functional $\mathcal{F} : \mathcal{D} \rightarrow \mathbb{R}$ at $\rho_0 \in \mathcal{D}$ as the infimum of \mathcal{F} and a penalty term,

$$\mathcal{F}^\varepsilon(\rho_0) = \inf_{\rho \in \mathcal{D}} \left\{ \mathcal{F}(\rho) + \frac{1}{2\varepsilon} \|\rho - \rho_0\|_{\mathcal{D}}^2 \right\}, \quad (1)$$

where $\varepsilon > 0$ is the regularization parameter. We refer to Eq. (1) as an *infimal convolution*. Our further discussion will be limited to the case when \mathcal{F} is a convex and lower semicontinuous functional [56] and \mathcal{D} a uniformly convex space (in fact a Hilbert space, but *not* identified with its dual). If $\mathcal{F} = F$ is the exact universal functional, then the (exact) ground-state energy, $E(v)$, of some external potential, v , can still be computed from F^ε using [49]

$$\begin{aligned} E^\varepsilon(v) &= \inf_{\rho \in \mathcal{D}} \{F^\varepsilon(\rho) + \langle v, \rho \rangle\}, \\ E(v) &= E^\varepsilon(v) + \frac{\varepsilon}{2} \|v\|_{\mathcal{V}}^2. \end{aligned}$$

This is a consequence of F^ε being an infimal convolution and of E which is the Fenchel conjugate of F . In this regard, regularizing F with the MY transform is *lossless* as far as the energy is concerned.

We consider systems which are periodic on a lattice with a unit cell denoted by $\Omega \subset \mathbb{R}^3$. The function spaces of interest are the periodic Sobolev spaces $H_{\text{per}}^s(\Omega, \mathbb{C})$, $s = \pm 1$, equipped with the norm $\|u\|_{H_{\text{per}}^s}^2 = \sum_{\mathbf{G}} (1 + |\mathbf{G}|^2)^s |\hat{u}_{\mathbf{G}}|^2$, where the sum is over the usual reciprocal lattice vectors \mathbf{G} [57, Sec. 2]. Henceforth, we assume that the densities ρ are elements of $\mathcal{D} = H_{\text{per}}^{-1}$ such that the potentials v are in $\mathcal{V} = H_{\text{per}}^1$. Denote by $J : \mathcal{D} \rightarrow \mathcal{V}$ the duality mapping, i.e., the canonical map from the primary space to its dual. In the particular setting considered here, the duality mapping $J(\rho)$ is the convolution

of the density ρ with the Yukawa potential [58], which is of importance when calculating the MY regularization.

In the interest of an inversion algorithm, suppose we are given some accurate (and fixed) ground state density ρ_{gs} for some periodic system of interacting particles. Moreover, assume that this density is non-interacting v -representable, i.e., there exist a potential for which ρ_{gs} is also a non-interacting ground-state density. In practice, ρ_{gs} could be obtained from various sources, e.g., experimental data, full configuration interaction [59], coupled-cluster [26], or quantum Monte-Carlo [18, 23, 60] calculations. The goal is then to obtain the one-body potential of the associated KS system, in which the aforementioned xc potential v_{xc} is the critical unknown. Let $\mathcal{F}(\rho) = T(\rho) + E_{\text{H}}(\rho) + \int_{\Omega} v_{\text{ext}} \rho$ be our guiding density functional built up from the *kinetic-only* constrained-search functional $T(\rho)$ [61, Eq. 3.17], Hartree contribution E_{H} , and the fixed external potential v_{ext} . The key optimization problem of our inversion scheme is the minimization over $\rho \in \mathcal{D}$ of

$$\mathcal{E}(\rho; \rho_{\text{gs}}) = \mathcal{F}(\rho) + \frac{1}{2\varepsilon} \|\rho - \rho_{\text{gs}}\|_{\mathcal{D}}^2. \quad (2)$$

The functional $\rho \mapsto \mathcal{E}(\rho; \rho_{\text{gs}})$ is convex and lower semicontinuous on the Hilbert space \mathcal{D} and the minimum is attained at a unique point $\rho_{\text{gs}}^\varepsilon = \text{argmin}_{\rho} \mathcal{E}(\rho; \rho_{\text{gs}})$ [62], referred to as the proximal density of ρ_{gs} . In the limit $\varepsilon \rightarrow 0^+$, it holds that $\rho_{\text{gs}}^\varepsilon \rightarrow \rho_{\text{gs}}$ [62, Prop. 1.146]. Since $\frac{\partial}{\partial \rho} \|\rho\|_{\mathcal{D}}^2 = 2\rho$, we have the stationary condition $\frac{\partial}{\partial \rho} \mathcal{F}(\rho_{\text{gs}}^\varepsilon) + \frac{1}{\varepsilon} J(\rho_{\text{gs}}^\varepsilon - \rho_{\text{gs}}) \ni 0$ for the minimization of \mathcal{E} . Here $\frac{\partial}{\partial \rho} \mathcal{F}$ denotes the subdifferential of \mathcal{F} and is the collection of all tangent functionals of \mathcal{F} . Under the assumption that the zero element of \mathcal{V} belongs to the set $\frac{\partial}{\partial \rho} \mathcal{F}(\rho_{\text{gs}}) + v_{\text{xc}}$ for some v_{xc} (i.e., the assumption of non-interacting v -representability), we obtain v_{xc} as the limit of $v_{\text{xc}}^\varepsilon = \frac{1}{\varepsilon} J(\rho_{\text{gs}}^\varepsilon - \rho_{\text{gs}})$ as $\varepsilon \rightarrow 0^+$ [47, Thm. 2]. For our choice of function spaces, this implies that

$$v_{\text{xc}}(\mathbf{r}) = \lim_{\varepsilon \rightarrow 0^+} \frac{1}{\varepsilon} \int_{\mathbb{R}^3} \frac{\rho_{\text{gs}}^\varepsilon(\mathbf{r}') - \rho_{\text{gs}}(\mathbf{r}')}{4\pi|\mathbf{r} - \mathbf{r}'|} e^{-|\mathbf{r} - \mathbf{r}'|} d^3r'. \quad (3)$$

In the setting presented here, the proximal mapping $\rho \mapsto \rho^\varepsilon$ is a (firmly [63]) non-expansive operator. To demonstrate this, we slightly generalize the proof of Prop. 2.3 in [64] to the case considered here, i.e., Hilbert spaces not identified with their duals. From the general fact that $-\frac{1}{\varepsilon} J(\rho^\varepsilon - \rho)$ is an element of $\frac{\partial}{\partial \rho} \mathcal{F}(\rho^\varepsilon)$, it follows that the set $\mathcal{A} := \varepsilon (\frac{\partial}{\partial \rho} \mathcal{F}(\rho^\varepsilon) - \frac{\partial}{\partial \rho} \mathcal{F}(\tilde{\rho}^\varepsilon))$ is included in the set difference $J(\rho - \tilde{\rho}) - J(\tilde{\rho} - \tilde{\rho}^\varepsilon)$. By the linearity of J , we have $\mathcal{A} + J(\rho^\varepsilon - \tilde{\rho}^\varepsilon) \ni J(\rho - \tilde{\rho})$. Then taking the dual pairing with $\rho^\varepsilon - \tilde{\rho}^\varepsilon$ yields

$$\|\rho^\varepsilon - \tilde{\rho}^\varepsilon\|_{\mathcal{D}}^2 \leq \langle J(\rho - \tilde{\rho}), \rho^\varepsilon - \tilde{\rho}^\varepsilon \rangle, \quad (4)$$

where we have used the maximal monotonicity [65] of the subdifferential of \mathcal{F}^ε and that $\langle J(\rho), \rho \rangle = \|\rho\|_{\mathcal{D}}^2$. Using Hölder's inequality,

$$\|\rho^\varepsilon - \tilde{\rho}^\varepsilon\|_{\mathcal{D}} \leq \|\rho - \tilde{\rho}\|_{\mathcal{D}}, \quad (5)$$

which establishes the non-expansiveness. Indeed, Eq. (4) proves the *firm* non-expansiveness [63].

For the purpose of further investigations, let us define $\|\rho^\varepsilon - \tilde{\rho}^\varepsilon\|_{\mathcal{D}} / \|\rho - \tilde{\rho}\|_{\mathcal{D}} = Q_\varepsilon(\rho, \tilde{\rho}) \leq 1$. The ratio satisfies $Q_\varepsilon \rightarrow 1$ as $\varepsilon \rightarrow 0^+$, by the fact that $\rho^\varepsilon \rightarrow \rho$. Equation (5) gives an estimate at a fixed $\varepsilon > 0$ for the error when performing the inversion using a perturbed density $\tilde{\rho}_{\text{gs}} = \rho_{\text{gs}} + \Delta\rho$ rather than the exact reference ρ_{gs} . The total error introduced in v_{xc} by using a $\tilde{\rho}_{\text{gs}}$ and terminating the inversion at an $\varepsilon > 0$ is by the triangle inequality

$$\|v_{\text{xc}} - \tilde{v}_{\text{xc}}^\varepsilon\|_{\mathcal{V}} \leq \|v_{\text{xc}} - v_{\text{xc}}^\varepsilon\|_{\mathcal{V}} + \|v_{\text{xc}}^\varepsilon - \tilde{v}_{\text{xc}}^\varepsilon\|_{\mathcal{V}}.$$

The first term is the error arising from terminating the inversion at $\varepsilon > 0$. This term is guaranteed to vanish as $\varepsilon \rightarrow 0^+$ [47, Thm. 2] and will be negligible for sufficiently small ε , a behaviour also seen in our numerical calculations, discussed below. Of interest for this Letter is the second term, sometimes referred to as a *density-driven* error [66–68]. Using that $v_{\text{xc}}^\varepsilon = \frac{1}{\varepsilon} J(\rho_{\text{gs}}^\varepsilon - \rho_{\text{gs}})$ and similarly for $\tilde{v}_{\text{xc}}^\varepsilon$, our main error bound,

$$\|v_{\text{xc}}^\varepsilon - \tilde{v}_{\text{xc}}^\varepsilon\|_{\mathcal{V}} \leq \frac{1 + Q_\varepsilon(\Delta\rho)}{\varepsilon} \|\Delta\rho\|_{\mathcal{D}}, \quad (6)$$

follows from the linearity of J , the triangle inequality, and Eq. (5). Note that the right-hand side can be universally bounded by $\frac{2}{\varepsilon} \|\Delta\rho\|_{\mathcal{D}}$, i.e., the error in potential is small in the regime $\|\Delta\rho\|_{\mathcal{D}} \ll \varepsilon$. To be able to further investigate Q_ε , we also note that

$$\|v_{\text{xc}}^\varepsilon - \tilde{v}_{\text{xc}}^\varepsilon - \frac{1}{\varepsilon} J(\Delta\rho)\|_{\mathcal{V}} \leq \frac{1}{\varepsilon} Q_\varepsilon(\Delta\rho) \|\Delta\rho\|_{\mathcal{D}} \quad (7)$$

holds. Let $R_\varepsilon(\Delta\rho)$ and $S_\varepsilon(\Delta\rho)$ be defined as the left-hand sides of Eqs. (6) and (7), respectively, multiplied by ε and divided by $\|\Delta\rho\|_{\mathcal{D}}$. Using $\|J(\Delta\rho)\|_{\mathcal{V}} / \|\Delta\rho\|_{\mathcal{D}} = 1$, the reverse triangle inequality applied to Eq. (7) gives $|R_\varepsilon - 1| \leq Q_\varepsilon$, i.e.,

$$0 \leq 1 - Q_\varepsilon(\Delta\rho) \leq R_\varepsilon(\Delta\rho) \leq 1 + Q_\varepsilon(\Delta\rho) \leq 2. \quad (8)$$

Moreover, Eq. (7) implies that $0 \leq S_\varepsilon \leq Q_\varepsilon \leq 1$. Given the above, we remark that Q_ε is a central quantity in our error analysis.

We next numerically demonstrate the presented inversion scheme and verify its error bounds (Eqs. (6) to (8)) by calculations on bulk silicon. The practical implementation of the $\varepsilon \rightarrow 0^+$ limit is performed in the following way: for an exponentially decreasing sequence in ε , the proximal density of ρ_{gs} is computed and $v_{\text{xc}}^\varepsilon$ is extracted by application of the duality mapping. As ε decreases, the expectation is that $v_{\text{xc}}^\varepsilon$ converges numerically to v_{xc} . The uniqueness of the proximal density for a fixed $\varepsilon > 0$ implies that $\rho_{\text{gs}}^\varepsilon$ can be obtained from \mathcal{E} by any minimization method of choice. To match the usual KS setting we employ a parametrization of the proximal density in terms of orthonormal orbitals and minimise \mathcal{E} using a BFGS-based quasi-Newton scheme [69, 70]. All applications of the duality mapping to $\rho_{\text{gs}}^\varepsilon - \rho_{\text{gs}}$ are computed

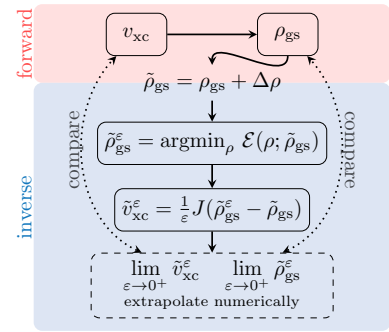


Figure 1. An illustration of the Moreau-Yosida (MY) inversion scheme. Given v_{xc} , a ground-state density ρ_{gs} is first computed in a forward, reference calculation. Here, $\Delta\rho$ represent an introduced error, resulting in an inexact reference density $\tilde{\rho}_{\text{gs}}$. For this $\tilde{\rho}_{\text{gs}}$, the proximal point $\tilde{\rho}_{\text{gs}}^\varepsilon$ is found from the MY regularization. An ε -dependent potential is then found by means of the duality mapping J , whereupon the potential is obtained by taking $\varepsilon \rightarrow 0^+$. The results of the inversion can then be compared with the forward scheme.

at increased precision using the `DoubleFloats.jl` [71] package. The optimization is stopped either if the optimizer has been obtained to machine precision or if the change in $\rho_{\text{gs}}^\varepsilon$ between two iterations drops below 0.01ε . Here, this heuristic criterion yields a good compromise between the required computational time and the accuracy of $v_{\text{xc}}^\varepsilon$ as well as an excellent agreement with our theoretical error bounds. We defer an investigation of a more efficient stopping criterion to future work. Further details on the numerical procedure can be found on GitHub [72], where the source code to reproduce the numerical results and all figures are available.

For obtaining our numerical results we follow the procedure outlined in Fig. 1. From an xc potential v_{xc} , we generate a reference ground-state density ρ_{gs} by solving the forward KS self-consistent field problem employing the PBE xc functional [73] (Fig. 1, red panel). The obtained density we feed to the KS inversion procedure described in the previous paragraph (Fig. 1, blue panel). For the purpose of investigating error bounds, controlled perturbations $\Delta\rho$ to the density ρ_{gs} are considered, as detailed below. The extrapolated proximal density along with the extrapolated xc potential can be directly compared to the respective quantities ρ_{gs} and v_{xc} obtained in the forward calculation. This setup, where the same quantum-chemical model and discretization basis is employed for both the inversion and the forward calculation is referred to as an *inverse crime* in the literature [32, 40, 74]. However, we remark that our main focus is to highlight the strict mathematical results offered by the MY inversion scheme. Therefore, it is beneficial to be able to compare both density and potential from the inversion procedure against the reference from the forward scheme.

First we consider the case of an “exact” inversion: we apply no additional noise ($\Delta\rho = 0$) and expect our in-

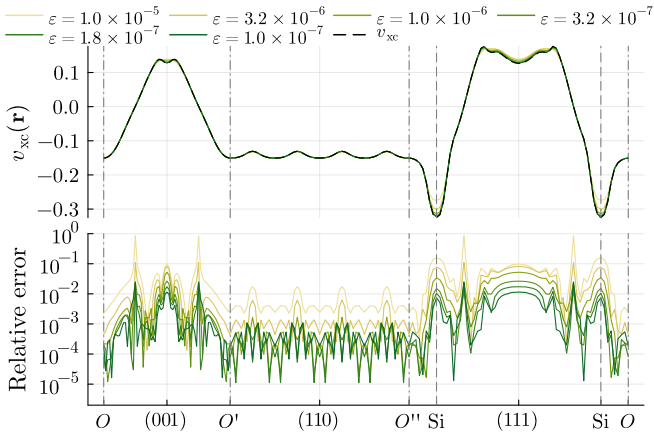


Figure 2. (top) Real-space plot of the reference xc potential along with the potential obtained from inversions for different values of the regularization parameter ϵ for bulk silicon. The potential is displayed along a closed path intersecting the high symmetry points [75, 76]. (bottom) The associated point-wise relative error of the potentials obtained from inversions at various ϵ compared to the reference xc potential.

version scheme to fully recover the xc potential. Figure 2 shows the resulting potentials, which are traced along the closed path in the unit cell suggested by Chen *et al.* [75, 76]. The top panel contrasts the reference v_{xc} against the potentials obtained from the inversion at selected values of ϵ . The bottom panel shows the point-wise absolute relative error of v_{xc}^ϵ against the reference v_{xc} . Two important features are observed. (1) Our inversion procedure accurately recovers the potential numerically: relative errors are below the 10 percentile for $\epsilon \sim 10^{-6}$, and decrease by another order of magnitude by reducing ϵ by an order of magnitude. (2) Near the sharpest features of the potential, the point-wise convergence in ϵ is slower and the relative errors larger.

To numerically study the susceptibility of the inversion algorithm to errors in the reference ground state density, ρ_{gs} , recall our notation $\tilde{\rho}_{gs} = \rho_{gs} + \Delta\rho$ for an inexact density. In practice, the erroneous part of the density, $\Delta\rho$, may arise from various sources depending on the origin of ρ_{gs} , e.g., basis truncations, change of basis, insufficiently converged reference densities, and experimental inaccuracies. Here, we limit ourselves to perturbations arising from an interpolation of the density utilizing a smaller plane-wave basis. Our numerical calculations show that such perturbations to the reference density do not alter the convergence properties of the potential as long as $\epsilon > \|\Delta\rho\|_{L_{per}^2}$. For smaller ϵ the potential starts diverging from the reference in \mathcal{V} -norm.

By comparing the proximal densities of ρ_{gs} and that of $\tilde{\rho}_{gs}$, we can investigate the non-expansiveness of the proximal mapping by computing the ratio $Q_\epsilon(\Delta\rho)$. A plot of Q_ϵ is shown in Fig. 3, where we have computed $\|\Delta\rho\|_{\mathcal{D}}$ for each truncation to give the absolute size of the perturbation. By the proximal map, Q_ϵ is bounded to the range $[0, 1]$. From Fig. 3 we see that for large val-

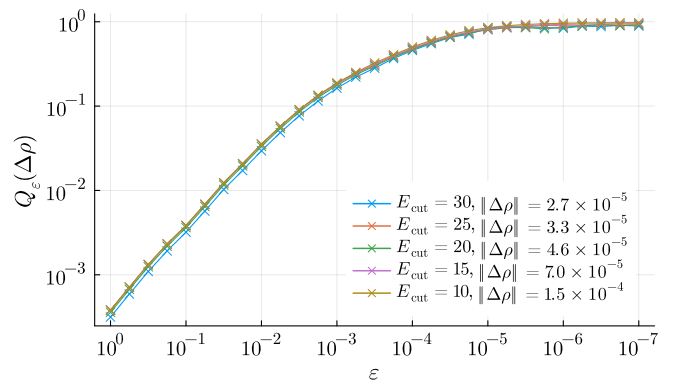


Figure 3. Related to the non-expansiveness of the proximal map, the ratio $Q_\epsilon(\Delta\rho) = \|\rho_{gs}^\epsilon - \tilde{\rho}_{gs}^\epsilon\|_{\mathcal{D}} / \|\Delta\rho\|_{\mathcal{D}}$ is here shown for a decreasing sequence in ϵ . The plot demonstrates the convergence of $Q_\epsilon \rightarrow 1$ as $\epsilon \rightarrow 0^+$ numerically.

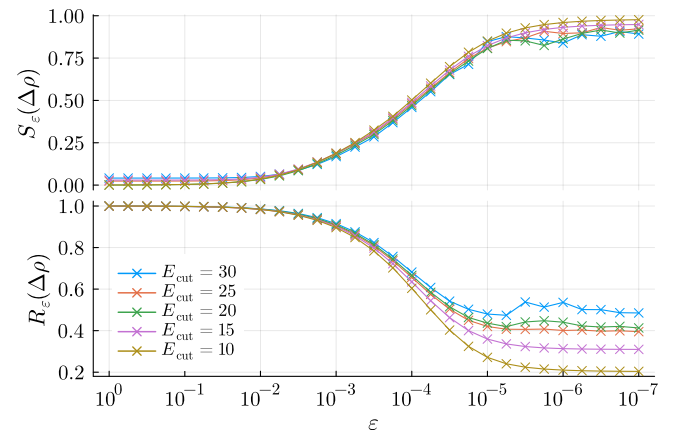


Figure 4. The ratios S_ϵ and R_ϵ as a function of ϵ for various basis truncations whose $\|\Delta\rho\|$ are given in Fig. 3. (top) S_ϵ , a mathematical equivalent measure to Q_ϵ , is small for large values of ϵ and increases to one as $\epsilon \rightarrow 0$. (bottom) For large ϵ -values R_ϵ is similar to one, and approaches its lower bound (8) as $\epsilon \rightarrow 0$. For $\epsilon \lesssim 5 \times 10^{-6}$ the problem becomes numerically challenging, which manifests in small oscillations in the trends of both quantities.

ues of the regularization parameter ($\epsilon \sim 1$) $Q_\epsilon \ll 1$, and $Q_\epsilon \rightarrow 1^-$ as $\epsilon \rightarrow 0^+$. Additionally, we may obtain estimates for the error bounds on the xc potential, Eqs. (6) and (7), directly from the ratios R_ϵ and S_ϵ . In particular, Fig. 4 shows the ratios R_ϵ and S_ϵ (respectively bottom and top panels) obtained using the same $\tilde{\rho}_{gs}$ as in Fig. 3. Furthermore, Fig. 4 (top) shows that the ratio S_ϵ depend on ϵ in a very similar manner as Q_ϵ (see Fig. 3). Note that for large values of ϵ the ratio S_ϵ does not adhere exactly to the bound $S_\epsilon \leq Q_\epsilon$ (Eq. (7)). However, this is not surprising given that it is obtained from the difference of three quantities that should point-wise be almost zero. For small values of ϵ , on the other hand, S_ϵ is in excellent agreement with bound set by Q_ϵ , also satisfying $S_\epsilon \rightarrow 1$ as $\epsilon \rightarrow 0^+$. Moreover, Fig. 4 (bottom) shows that the ratio R_ϵ adheres strictly to the bound set by Q_ϵ (Eq. (6)). In particular, R_ϵ follow closely the lower bound $R_\epsilon \geq 1 - Q_\epsilon$ (Eq. (8)). Although obtaining the

ratios involved in the error bounds, Eqs. (6) to (8), is not computationally feasible in practical calculations, our numerical results conform to the theoretical predictions. In fact, Figs. 3 and 4 even indicate that the ratio Q_ε may be estimated by a constant independent of $\Delta\rho$, but parametrically dependent on ε (and the density functional). Theoretically exploring this observation further marks an extremely promising direction for future research towards more approximate bounds, which could be applied within a practical inversion scheme to make it more efficient and reliable.

In this Letter we set the stage for further in-depth numerical analyses of KS inversion. Facing the challenges of numerically solving the many-body electronic-structure problem, progress is often the result from combining insights from mathematical analysis, more efficient numerical schemes as well as physically sound approximations. We have shown that the theoretical error bounds, Eqs. (6) to (8), as well as the non-expansiveness, Eq. (5), are manifested in our numerical calculations. Whilst our numerical study in this first work is restricted to bulk silicon, this is not a fundamental limitation of neither theory nor implementation. Since the calculations have been performed in a general DFT code with demonstrated performance on systems up to a few hundred electrons, a generalization to more involved systems is possible and aspired for. Future works should also aim to apply our presented inversion scheme to densities obtained from accurate sources other than forward KS algorithms. The inversion scheme, the explicit form of v_{xc} (Eq. (3)), the non-expansiveness of the proximal map, and the error bounds on the inverted potential are all novel theoretical results that are also numerically demonstrated. These results establish mathematical guarantees for KS inversion not previously seen, and also mark the first successful application of the MY framework to a physical system. We believe that such mathematical results, closely accompanied with numerical calculations, will significantly aid the development of more reliable KS inversion schemes. Moreover, the first stringent error bounds presented here open a new avenue for developing rigorous error estimates for density-potential inversion problems. Strengthened KS inversion schemes, in union with error analysis, should ultimately further the development of approximate density functionals. Furthermore, as highlighted in [40], such enhanced understanding of density-potential inversion may lead to advances in explorations of the Hohenberg–Kohn mapping, quantum embedding techniques, and enhanced optimised effective potentials.

Acknowledgments. AL and VHB were supported by ERC-2021-STG grant agreement No. 101041487. AL was also supported by RCN through CoE Hylleraas Centre for Quantum Molecular Sciences Grant No. 262695 and CCError Grant No. 287906. MFH acknowledges support by the NCCR MARVEL, a National Centre of Competence in Research, funded by the Swiss National

Science Foundation (Grant No. 205602). MFH and AL thank the Oberwolfach Research Institute for Mathematics where part of this research was conducted. We express our gratitude for fruitful discussions with N. Marzari and M. Penz.

* michael.herbst@epfl.ch

† andre.laestadius@oslomet.no

- [1] K. Burke, *J. Chem. Phys.* **136** (2012).
- [2] P. Verma and D. G. Truhlar, *Trends in Chemistry* **2**, 302 (2020), special Issue - Laying Groundwork for the Future.
- [3] A. M. Teale et al., *Phys. Chem. Chem. Phys.* **24**, 28700 (2022).
- [4] P. Hohenberg and W. Kohn, *Phys. Rev.* **136**, B864 (1964).
- [5] N. Schuch and F. Verstraete, *Nature Physics* **5**, 732–735 (2009).
- [6] W. Kohn and L. J. Sham, *Phys. Rev.* **140**, A1133 (1965).
- [7] J. Toulouse, “Review of approximations for the exchange-correlation energy in density-functional theory,” in *Density Functional Theory: Modeling, Mathematical Analysis, Computational Methods, and Applications*, edited by E. Cancès and G. Friesecke (Springer International Publishing, Cham, 2023) pp. 1–90.
- [8] A. J. Cohen, P. Mori-Sánchez, and W. Yang, *Science* **321**, 792 (2008).
- [9] D. G. Tempel, T. J. Martínez, and N. T. Maitra, *J. Chem. Theory Comput.* **5**, 770 (2009).
- [10] N. Helbig, I. V. Tokatly, and A. Rubio, *J. Chem. Phys.* **131**, 224105 (2009).
- [11] L. J. Sham and M. Schlüter, *Phys. Rev. Lett.* **51**, 1888 (1983).
- [12] L. J. Sham and M. Schlüter, *Phys. Rev. B* **32**, 3883 (1985).
- [13] J. P. Perdew, R. G. Parr, M. Levy, and J. L. Balduz, *Phys. Rev. Lett.* **49**, 1691 (1982).
- [14] J. P. Perdew and M. Levy, *Phys. Rev. Lett.* **51**, 1884 (1983).
- [15] M. Grüning, A. Marini, and A. Rubio, *J. Chem. Phys.* **124**, 154108 (2006).
- [16] N. Mardirossian and M. Head-Gordon, *Molecular Physics* **115**, 2315 (2017).
- [17] F. Aryasetiawan and M. J. Stott, *Phys. Rev. B* **38**, 2974 (1988).
- [18] W. Knorr and R. W. Godby, *Phys. Rev. Lett.* **68**, 639 (1992).
- [19] A. Görling, *Phys. Rev. A* **46**, 3753 (1992).
- [20] Q. Zhao and R. G. Parr, *J. Chem. Phys.* **98**, 543 (1993).
- [21] Y. Wang and R. G. Parr, *Phys. Rev. A* **47**, R1591 (1993).
- [22] Q. Zhao, R. C. Morrison, and R. G. Parr, *Phys. Rev. A* **50**, 2138 (1994).
- [23] W. Knorr and R. W. Godby, *Phys. Rev. B* **50**, 1779 (1994).
- [24] R. van Leeuwen and E. J. Baerends, *Phys. Rev. A* **49**, 2421 (1994).
- [25] W. Yang and Q. Wu, *Phys. Rev. Lett.* **89**, 143002 (2002).
- [26] Q. Wu and W. Yang, *J. Chem. Phys.* **118**, 2498 (2003).
- [27] K. Peirs, D. Van Neck, and M. Waroquier, *Phys. Rev. A* **67**, 012505 (2003).
- [28] E. S. Kadantsev and M. J. Stott, *Phys. Rev. A* **69**, 012502 (2004).

- (2004).
- [29] F. A. Bulat, T. Heaton-Burgess, A. J. Cohen, and W. Yang, *J. Chem. Phys.* **127**, 174101 (2007).
- [30] A. P. Gaiduk, I. G. Ryabinkin, and V. N. Staroverov, *J. Chem. Theory Comput.* **9**, 3959 (2013).
- [31] L. O. Wagner, T. E. Baker, E. M. Stoudenmire, K. Burke, and S. R. White, *Phys. Rev. B* **90**, 045109 (2014).
- [32] D. S. Jensen and A. Wasserman, *Int J Quantum Chem.* **118** (2018).
- [33] X. Zhang and E. A. Carter, *J. Chem. Phys.* **148**, 034105 (2018).
- [34] Q. Ou and E. A. Carter, *J. Chem. Theory Comput.* **14**, 5680 (2018).
- [35] A. Kumar, R. Singh, and M. K. Harbola, *J. Phys. B* **52**, 075007 (2019).
- [36] B. Kanungo, P. M. Zimmerman, and V. Gavini, *Nat Commun* **10**, 4497 (2019).
- [37] A. Kumar and M. K. Harbola, *Int J Quantum Chem.* **120**, e26400 (2020).
- [38] R. Garrick, A. Natan, T. Gould, and L. Kronik, *Phys. Rev. X* **10**, 021040 (2020).
- [39] T. J. Callow, N. N. Lathiotakis, and N. I. Gidopoulos, *J. Chem. Phys.* **152**, 164114 (2020).
- [40] Y. Shi and A. Wasserman, *J. Phys. Chem. Lett.* **12**, 5308 (2021).
- [41] J. Erhard, E. Trushin, and A. Görling, *J. Chem. Phys.* **156**, 204124 (2022).
- [42] T. Gould, *J. Chem. Phys.* **158**, 064102 (2023).
- [43] S. Nam, R. J. McCarty, H. Park, and E. Sim, *J. Chem. Phys.* **154**, 124122 (2021).
- [44] Y. Shi, V. H. Chávez, and A. Wasserman, *WIREs Comput Mol Sci.* **12**, e1617 (2022).
- [45] S. Crisostomo, R. Pederson, J. Kozłowski, B. Kalita, A. C. Cancio, K. Datchev, A. Wasserman, S. Song, and K. Burke, *Lett Math Phys* **113** (2023).
- [46] J. Wrighton, A. Albavera-Mata, H. F. Rodríguez, T. S. Tan, A. C. Cancio, J. W. Dufty, and S. B. Trickey, *Lett Math Phys* **113** (2023).
- [47] M. Penz, M. A. Csirik, and A. Laestadius, *Electron. Struct.* **5**, 014009 (2023).
- [48] S. Kvaal, U. Ekström, A. M. Teale, and T. Helgaker, *J. Chem. Phys.* **140**, 18A518 (2014).
- [49] A. Laestadius, M. Penz, E. I. Tellgren, M. Ruggenthaler, S. Kvaal, and T. Helgaker, *J. Chem. Phys.* **149**, 164103 (2018).
- [50] A. Laestadius, E. I. Tellgren, M. Penz, M. Ruggenthaler, S. Kvaal, and T. Helgaker, *J. Chem. Theory Comput.* **15**, 4003 (2019).
- [51] M. Penz, A. Laestadius, E. I. Tellgren, and M. Ruggenthaler, *Phys. Rev. Lett.* **123**, 037401 (2019).
- [52] M. Penz, A. Laestadius, E. I. Tellgren, M. Ruggenthaler, and P. E. Lammert, *Phys. Rev. Lett.* **125**, 249902(E) (2020).
- [53] P. E. Lammert, *Int. J. Quantum Chem.* **107**, 1943 (2007).
- [54] M. F. Herbst, A. Levitt, and E. Cancès, *Proceedings of the JuliaCon Conference* **3**, 69 (2021).
- [55] In particular, obtaining the ground-state density ρ is equivalent to saturating the Fenchel–Young inequality $E(v) \leq \mathcal{F}(\rho) + \langle v, \rho \rangle$.
- [56] A set S is convex if the line segment $\lambda x + (1 - \lambda)y \in S$ whenever $x, y \in S$. A functional defined on a convex set S is convex if for all $x, y \in S$ and $\lambda \in (0, 1)$ we have $f(\lambda x + (1 - \lambda)y) \leq \lambda f(x) + (1 - \lambda)f(y)$. Moreover, f is lower semicontinuous if $f(x) \leq \liminf_{y \rightarrow x} f(y)$ whenever $y \rightarrow x$.
- [57] E. Cancès, R. Chakir, and Y. Maday, *ESAIM: Mathematical Modelling and Numerical Analysis* **46**, 341 (2012).
- [58] By definition the duality mapping, given the particular choice of vector spaces $\mathcal{D} = H_{\text{per}}^{-1}$ and $\mathcal{V} = H_{\text{per}}^1$ ($J : \mathcal{D} \rightarrow \mathcal{V}$), can be written as
- $$J(\rho) = \sum_{\mathbf{G}} \frac{\hat{\rho}_{\mathbf{G}} e_{\mathbf{G}}}{1 + |\mathbf{G}|^2}.$$
- Here $\hat{\rho}_{\mathbf{G}}$ are the Fourier coefficients of ρ and $e_{\mathbf{G}}$ the associated (normalized) basis vectors. It thus follows from a direct calculation that $J[\rho](\mathbf{r}) = (\Phi * \rho)(\mathbf{r})$, $\forall \mathbf{r} \in \Omega$, where $\Phi(\mathbf{r}) = \exp(-|\mathbf{r}|)/(4\pi|\mathbf{r}|)$.
- [59] S. Tribedi, D.-K. Dang, B. Kanungo, V. Gavini, and P. M. Zimmerman, *J. Chem. Phys.* **159**, 054106 (2023).
- [60] A. Aouina, M. Gatti, S. Chen, S. Zhang, and L. Reining, *Phys. Rev. B* **107**, 195123 (2023).
- [61] E. H. Lieb, *Int. J. Quantum Chem.* **24**, 243 (1983).
- [62] V. Barbu and T. Precupanu, *Convexity and Optimization in Banach Spaces*, 4th ed., Springer Monographs in Mathematics (Springer Netherlands, 2012).
- [63] We use the notion of a firmly non-expansive operator as in the case of a Hilbert space identified with its dual with the obvious inclusion of the duality mapping, i.e., Eq. (4).
- [64] V. Barbu, *Nonlinear Differential Equations of Monotone Types in Banach Spaces*, 1st ed., Springer Monographs in Mathematics (Springer New York, 2010).
- [65] A set $A \subset X \times X^*$ is said to be monotone if
- $$\langle y_1 - y_2, x_1 - x_2 \rangle \geq 0 \quad \forall [x_i, y_i] \in A, i = 1, 2,$$
- and maximally monotone if the set is not properly contained in any other monotone subset of $X \times X^*$ [64, Def. 2.1] By the lower semicontinuity of the subdifferential of a convex functional, the maximal monotonicity follows.
- [66] M.-C. Kim, E. Sim, and K. Burke, *Phys. Rev. Lett.* **111**, 073003 (2013).
- [67] S. Nam, S. Song, E. Sim, and K. Burke, *J. Chem. Theory Comput.* **16**, 5014–5023 (2020).
- [68] A. D. Kaplan, C. Shahi, P. Bhetwal, R. K. Sah, and J. P. Perdew, *J. Chem. Theory Comput.* **19**, 532 (2023).
- [69] A. Edelman, T. A. Arias, and S. T. Smith, *SIAM J. Matrix Anal. Appl.* **20**, 303 (1998).
- [70] N. Boumal, *Introduction to Optimization on Smooth Manifolds* (Cambridge University Press, 2023).
- [71] J. Sarnoff and JuliaMath, “Doublefloats,” (2024), juliamath.github.io/DoubleFloats.jl/stable.
- [72] github.com/mfherbst/supporting-my-inversion.
- [73] J. P. Perdew, K. Burke, and M. Ernzerhof, *Phys. Rev. Lett* **77**, 3865 (1996).
- [74] D. S. Jensen, *Density-to-Potential Inversions in Density Functional Theory*, Ph.D. thesis, Purdue University (2016).
- [75] S. Chen, M. Motta, F. Ma, and S. Zhang, *Phys. Rev. B* **103**, 075138 (2021).
- [76] Starting from O , the high-symmetry middle point between the two silicon atoms of a unit cell, we follow along the route $O - (001) - O' - (110) - O'' - (111) - O$, where O' and O'' denote the nearest symmetry-equivalent points to O along the respective path (following [75]).